

# End-to-end entanglement in Bose-Hubbard chains

Jose Reslen and Sougato Bose

*Dept. of Physics and Astronomy, University College London,  
Gower Street, WC1E 6BT London, United Kingdom*

(Dated: November 4, 2018)

We study the ground state as well as the dynamics of chains of bosons with local repulsive interactions and nearest-neighbour exchange using numerical techniques based on density matrix decimation. We explore the development of entanglement between the terminal sites of such chains as mechanisms are invoked to concentrate population in these sites. We find that long-range entanglement in the ground state emerges as a result of transfer taking place across the length of the whole chain in systems with appropriate hopping coefficients. Additionally, we find appropriate perturbations to increase the entanglement between the end sites above their ground state values.

## I. INTRODUCTION

As constant experimental developments expand our possibilities of materializing a new generation of computing devices, the need for a better understanding of quantum phenomena becomes more important. Outstanding emphasis has been placed on the concept of entanglement as, for example, a resource for quantum information processing and in general as a tool to study the contrast between classical and quantum physics. One fundamental problem that is now the subject of intensive research is the emergence of quantum correlations between distant sites of a quantum system. For most many-body systems this is notoriously difficult and entanglement between distant sites can only be achieved through clever engineering [1] or non-equilibrium dynamics [2, 3, 4, 5, 6], where, in the latter case, either intricate methodology is required or the amount of entanglement between the ends, though finite, is not substantial in amount. Typically, in quantum many-body systems, even when total correlations are long range, the entanglement between individual constituents such as spins is extremely short range, such as between nearest or next to nearest neighbours [7]. Thus it is already interesting when in some many-body system an entanglement between its farthest components, such as the spins or harmonic oscillators at the very ends of an open chain, can be generated and even more interesting when it is substantial in amount. Most of the work done in this field has been carried out in light-matter systems

and spin chains, but more recently, the development on new numerical techniques and algorithms [8] has opened the possibility of addressing more challenging scenarios such as chains of interacting bosons [5, 9, 10, 11]. Usually, where bosonic chains have been studied, though true quantum correlations have indeed been found to emerge between distant individual sites, they are generically not “substantial” in magnitude [2, 12]. Thus substantial entanglement between distant sites of a Bose-Hubbard model, even if with some reasonable engineering of the Hamiltonian, should be of great interest, not only because of the uncommon nature of such long distance entanglement, as motivated above, but also because from the practical point of view this entanglement is known to be “distillable”, i.e., convertible from an impure (mixed state) to a pure useful form through local actions. Density matrices whose partial transposes display negative eigenvalues are distillable [13] – so if one finds a mixed entangled state with the above property then, one can already claim, at least *in principle*, to have a resource for quantum communication.

Chains of bosons are more often than not well described by the Bose-Hubbard model [14, 15, 16]. In this model bosons can hop between neighbouring sites while undergoing local repulsion when several bosons occupy the same site. The development in atom cooling techniques has led to a significant rise in the amount of experiments related to the Bose-Hubbard model. The transition from a superfluid to a Mott insulator has been verified in numerous experiments of cold atoms in optical lattices as for example in Refs. [15, 17, 18, 19, 20], just to mention a few. As a result, physical realizations of quantum systems displaying key features such as long range entanglement is becoming more and more feasible. Motivated by these advances, in this paper we analyse from a fundamental point of view the emergence of long-range quantum correlations in Bose-Hubbard chains (Fig. 1). There has been one previous investigation on long range entanglement in a Bose-Hubbard chain where the dynamics is effectively reducible to a single particle propagation in a lattice [5]. Our study is, however, irreducibly a many-particle situation and can even result in more entanglement than what a single particle hopping in a lattice can ever do. It is also pertinent to point out

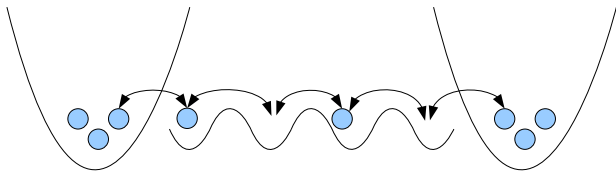


FIG. 1: Potential realization of a Bose-Hubbard chain in an optical lattice. The above finite lattice can be realized in one cell of a superlattice. The end sites of the lattice are depicted differently in the figure as we will require them to have vanishing repulsion in our study.

that there has been much interesting work on the various forms of entanglement contained in Bose gases [21, 22], but here we concentrate on a specific type of entanglement, namely that between two individual sites at the very ends. If implemented in the laboratory, the entanglement obtained from the scheme presented in this work, as it is distillable, would provide a resource for quantum information applications. In addition to the end-to-end entanglement, which has been motivated above, in this paper we will also present some results for the entanglement between a couple of other bi-partite partitions of the chain to fully appreciate the distribution of entanglement between parts of a finite chain as the strength of the local repulsion between bosons is varied.

## II. THE HUBBARD MODEL: CHARACTERISTICS AND METHODS

We assume a chain of size  $N$  with  $M$  bosons, nearest-neighbour hopping and open ended boundary conditions governed by a Bose-Hubbard Hamiltonian with variable coefficients,

$$\hat{H} = \sum_{k=1}^N \frac{U_k}{2} \hat{a}_k^\dagger \hat{a}_k (\hat{a}_k^\dagger \hat{a}_k - 1) - \sum_{k=1}^{N-1} J_k (\hat{a}_{k+1}^\dagger \hat{a}_k + \hat{a}_k^\dagger \hat{a}_{k+1}). \quad (1)$$

Constants  $U_k$  and  $J_k$  account for the on-site repulsion and hopping respectively while the annihilation and creation operators  $\hat{a}_k^\dagger$  and  $\hat{a}_k$  obey the usual commuting rules  $[\hat{a}_l, \hat{a}_k^\dagger] = \delta_k^l$  and  $[\hat{a}_k^\dagger, \hat{a}_l^\dagger] = [\hat{a}_k, \hat{a}_l] = 0$ . Physical realizations of this Hamiltonian include experiments where remarkable control of the ratio  $U/J$  can be achieved [15, 17, 20]. In a typical experiment, atoms are cooled in an optical lattice of retroreflected diode lasers and then transferred into a magnetic trap where further cooling is to take place. This creates an arrangement of atoms where the resulting optical potential depths  $V_{x,y,z}$  are proportional to the laser intensities and can be expressed in terms of the recoil energy  $E_R = \frac{\hbar k^2}{2m}$  with  $m$  the atomic mass and  $k$  the wavelength number. To prepare 1D arrays two lattice lasers are given high intensities in such a way that hopping can only efficiently take place across one axis [19]. In terms of experimental parameters, hopping and repulsion coefficients are given by  $J = A \left(\frac{V_0}{E_R}\right)^B e^{-C\sqrt{V_0/E_R}} E_R$  and  $U = \frac{2a_s E_R}{d} \sqrt{\frac{2\pi V_\perp}{E_R}} \left(\frac{V_0}{E_R}\right)^{\frac{1}{4}}$  where  $V_0$  is the axial lattice depth,  $V_\perp$  the depth of the lattice in the transverse directions,  $a_s$  the  $s$ -wave scattering length,  $d$  the lattice spacing and  $A$ ,  $B$  and  $C$  fixed constants [23, 24]. Spatial variations in  $U$  and  $J$  can also be implemented using detuned lasers sent through specific sections of the lattice as reported in Ref. [18].

From the Heisenberg equations of motion we know  $\frac{d\hat{a}_k}{dt} = ie^{-it\hat{H}}[\hat{a}_k^\dagger, \hat{H}]e^{it\hat{H}}$ , where  $\hat{a}_k = e^{-it\hat{H}}\hat{a}_k^\dagger e^{it\hat{H}}$ . In

the general case non-linearities induced mostly by repulsive terms keep us from getting reliable expressions for the  $\hat{a}_k$  in terms of time. One fortunate instance is the repulsionless case where all  $V_k$  go to zero and we are left with

$$\frac{d}{dt} \begin{pmatrix} \hat{a}_1 \\ \hat{a}_2 \\ \hat{a}_3 \\ \vdots \\ \hat{a}_N \end{pmatrix} = -i \begin{pmatrix} 0 & J_1 & 0 & \cdots & 0 \\ J_1 & 0 & J_2 & \cdots & 0 \\ 0 & J_2 & 0 & \cdots & 0 \\ \vdots & \vdots & \vdots & \ddots & J_{N-1} \\ 0 & 0 & 0 & J_{N-1} & 0 \end{pmatrix} \begin{pmatrix} \hat{a}_1 \\ \hat{a}_2 \\ \hat{a}_3 \\ \vdots \\ \hat{a}_N \end{pmatrix}. \quad (2)$$

One can of course assume that all the coupling constants are equal, which corresponds to the usually studied, and perhaps the most natural, setting of the Bose-Hubbard model. To contrast with this, one can also study a setting with non-uniform couplings to investigate whether better end to end entanglement can be obtained by appropriately engineering the couplings. As an example we will choose a non-uniform hopping distribution that matches an angular momentum representation of length  $j = \frac{N-1}{2}$ , namely  $J_k = \frac{\Delta}{2} \sqrt{k(N-k)}$  ( $\lambda = 2$  for all the simulations presented in this work). The above couplings, when present in spin chains, are known to facilitate a perfect quantum state transfer [25], which has been developed in context of the idea of using spin chains to convey quantum states [26]. In a Hubbard model, the above coupling profile will transfer particles perfectly from one end of the chain to the other [12] (however, the aim of this paper is different, namely generating entanglement between the ends). Moreover, because we are interested in studying end-to-end entanglement (EEE), hopping distributions are known to play a crucial role as it is particle tunnelling what determines how distant places get correlated with each other. So, in this work we compare results from two different hopping profiles, namely, the well known constant hopping (CH)  $J_k = 1$  and the above introduced perfect transmission hopping (PTH). The purpose in bringing in PTH is to explore what kind of physics is shown by a hopping profile with perfect transmission properties in situations where transport is either absent or not directly involved. The natural question in this context is whether perfect transmission properties, which involve dynamical synchronization at long scales, are in any way linked to the onset of quantum correlations among distant sites of a boson chain.

On the other hand, when repulsive terms in Eq. (1) are considered we apply numerical methods. Here we make use of density-matrix techniques as presented in [8], also known as *TEBD*, combined with conservation and symmetry properties associated with the Hamiltonian. Briefly, *TEBD* consists in writing the state in terms of canonical coefficients that are closely related to Schmidt vectors. These coefficients are updated through successive applications of semi-local unitary operations that correspondingly only modify coefficients associated with the sub-spaces on which they act. This fact is then skillfully exploited to work out an efficient way of simulating

both real and complex evolution. In addition to the standard set of coefficients  $\Gamma$  and  $\lambda$  employed in the canonical representation of the state, we also retain the number of particles associated with every Schmidt vector in the decomposition. Memory storage is handled by making use of allocatable types and pointers in FORTRAN 95, which suits the mechanics of TEBD where the dimension of the Hilbert space is updated adaptively. Usually, the TEBD coefficients that determine the local properties of the chain are presented with explicit reference to every local dimension, i.e.  $\Gamma_{\alpha\beta}^{[n]i}$ , where  $i = 1, \dots, M$ , being  $M$  the number of total number of bosons in the chain. However, the only relevant component  $i$  above is completely determined by the number of particles  $m_\alpha$  and  $m_\beta$  associated with Schmidt vectors  $|\alpha\rangle$  and  $|\beta\rangle$  in the expression  $|\psi\rangle = \sum_{\alpha,\beta,i} \Gamma_{\alpha\beta}^{[n]i} |\alpha\rangle |i\rangle |\beta\rangle$  through the relation  $m_\alpha + m_\beta + i = M$ . Consequently, truncating the local Hilbert space as a way of attenuating the memory requirement of the simulation is not necessary. Similarly, we use dynamical allocation and deallocation to store the canonical representation, which allows an efficient handling of computer memory. The maximum number of Schmidt coefficients  $\chi$  as well as the size of other elements relevant to the simulation are updated at run time. After every updating step we retain all the Schmidt coefficients greater than  $\lambda_1^i \times 10^{-14}$ , where  $\lambda_1^i$  is the greatest coefficient at site  $i$ . In ground state simulations,  $\chi$  saturates and remains quite fixed until the state converges (Insets in Fig. 8). For real time simulations, on the other hand, this convenient saturation does not manifest as strongly as in the ground state case and in some cases, specially for long simulations, truncation in the number of coefficients is important as a mean of sustaining the simulation efficiency. In our program we use second order Trotter expansion with time steps  $\delta t = \frac{10^{-3}}{N_e}$ , where  $N_e$  is the effective length of the chain, which is to be taken just as the number of sites in the chain unless something else be specified. Here we limit ourselves to Hamiltonians with symmetric distributions of parameters with respect to the centre of the chain and with an even number of sites and bosons. Additionally, all the simulations presented in this work correspond to  $M = N$ . Therefore, the system can be genuinely simulated by focusing on the canonical coefficients of half of the chain plus the interaction between complementary half-chain blocks. The algorithm is applied recursively to simulate  $|\psi_G\rangle = \lim_{\tau \rightarrow \infty} \frac{e^{-\tau \hat{H}} |\psi_0\rangle}{\|e^{-\tau \hat{H}} |\psi_0\rangle\|}$ , until convergence to the ground state  $|\psi_G\rangle$  is accomplished according to the criterion  $|1 - \langle \psi(\tau) | \psi(\tau + \delta\tau) \rangle| < 10^{-14}$ . Ground state simulations in repulsionless chains agree well with the exact ground state of Hamiltonian (1), which for PTH chains reads

$$\left( \sum_{m=-j}^j \frac{(-1)^{j+m}}{2^j} \sqrt{\frac{(2j)!}{(j-m)!(j+m)!}} \hat{a}_{m+j+1}^\dagger \right)^M \prod_{l=1}^N |0_l\rangle, \quad (3)$$

with energy  $E_G = -\lambda j N$ . Similar expressions for the

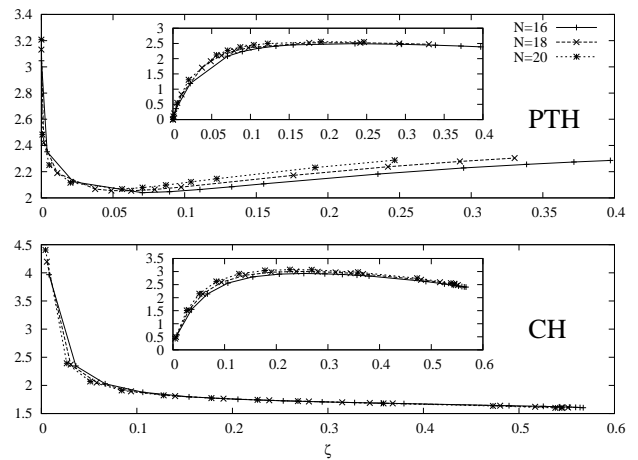


FIG. 2: Entanglement between both halves of the chain (main plots) and entanglement between the ends and the rest of the system (Insets). In PTH chains, when repulsion is sufficiently strong tunnelling starts to take place throughout the whole chain, enhancing the amount of entanglement in the system. CH chains, on the other hand, display an entanglement register that can be understood as being originated from short scope hopping.

ground state of CH chains can be found elsewhere. Additionally, real-time simulations coincide with available theoretical results [5, 12, 27].

As it was stated from the introduction of TEBD and further verified in several numerical studies [28], efficient simulations can be carried out as long as the state can be represented using reasonable low  $\chi$ , i.e., correlations are not too strong. As a reference one could take the infinity Hubbard model with unit filling, where such regime would correspond primarily to the Mott insulator phase where according to mean field theory  $\frac{U}{zJ} > 5.8$  with  $z = 2d$  the number of nearest neighbours [14, 15]. Another efficient simulation scenario corresponds to the case when, although hopping constants are strong and superfluid features dominate, the Hamiltonian structure remains close to integrability, e.g.  $\frac{U}{J} \ll 1$ , since usually integrable dynamics takes place in subspaces. When the case is neither of the above mentioned, as it is for most of the simulations presented from now on, one can still see that  $\chi$  often remains well below the maximum allowed in the Hilbert space.

### III. RESULTS

#### A. Ground state

In order to calculate the entanglement between the ends of the chain, we need to get the corresponding reduced density matrix. This task is by itself challenging, as the quantum state is given in terms of canonical coefficients associated with TEBD and not in the standard basis. Similarly, the computation of such density matrix

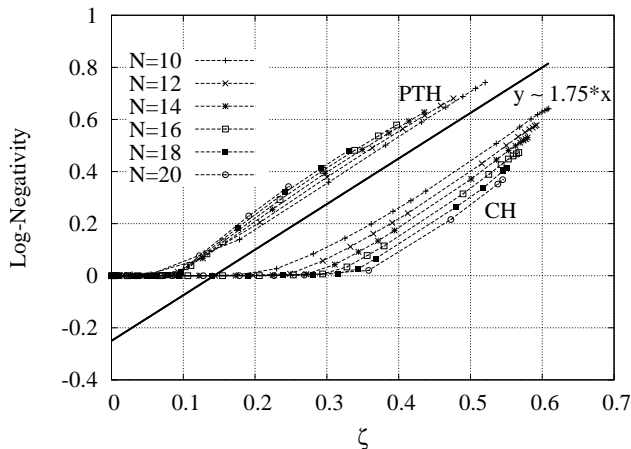


FIG. 3: The emergence of EEE in the chain as the on-site repulsion or equivalently the fractional population at the end sites  $\zeta$  is increased. Linear behaviour can be observed independently of the chain size. Also, EEE in chains with PTH lingers on when the size of the chain is increased, in contrast to EEE in CH chains.

is greatly improved in terms of speed and memory when exploiting number conservation. Once this density matrix is obtained, we have to quantify the entanglement using a measure which is appropriate for mixed states of two arbitrary dimensional quantum systems. So we choose the *logarithmic negativity* as defined in Ref. [29]. Moreover, to measure the entanglement between complementary subsystems [30], we use *von Neumann entropy*  $S = -\text{tr}(\hat{\rho}_A \log_2(\hat{\rho}_A))$  where  $\hat{\rho}_A$  represents the reduced density matrix of subsystem  $A$ . In this work we focus on chains with unit filling and open boundary conditions. Here we show results against the fraction of particles present on the ends  $\zeta = \frac{2\langle \hat{a}_1^\dagger \hat{a}_1 \rangle}{M}$  which allows a convenient depiction of the system phenomenology for different chain sizes.  $\zeta$  varies according to the intensity of the repulsion in intermediate sites. When repulsion is small, few particles remain on the ends and  $\zeta \approx 0$ . When repulsion is strong the amount of particles on the ends is maximum and  $\zeta = \frac{1}{2} + \frac{1}{M}$ .

Irrespective of the hopping profile the ground state of repulsionless chains is highly superfluid, although with most of the hopping taking place in the central part, leaving the terminal positions nearly unoccupied. In this repulsionless regime entanglement is strong, but confined around the centre. For example, in these circumstances, it is strong between the left and right halves of the chain. When repulsion in intermediate positions is increased, particles are forced to hop through longer distances and correlations develop at longer scales. Similarly, bosons accumulate on the terminals according to the strength of the interaction in intermediate places. Notice that on account of the repulsionless ends, particles can always find channels to hop, no matter how intense the repulsion in intermediate sites. Small repulsion leads to a decrease of entanglement between both halves and an increase of en-

tanglement between both ends and the rest of the system, an indication that entanglement is being spread along the chain following the particle distribution profile. When repulsion is increased even more, the terminals start getting macroscopically occupied while the average number of bosons in intermediate sites falls asymptotically towards  $\frac{1}{2}$ , which means that strong tunnelling renders the quantum state of intermediate places into a state that involves superpositions of kets corresponding to one or zero bosons. In this case correlations among places near the ends and in opposite sides of the chain are strongly enhanced, in contrast to the correlations in the centre of the chain. This can be seen in the inset plots of Fig. 2 where von Neumann entropy between both ends and the rest of the system slightly comes down after the original redistribution of entanglement mentioned above occurs. The emergence of EEE in the chain is shown in Fig. 3, which shows that as repulsion in the centre becomes intense, the terminals will tend to entangle with each other more strongly than with intermediate sites.

Once the conditions for the emergence of EEE are given, what determines how much entanglement can be generated is the hopping *scope*. Indeed, what is being really adjusted when repulsion is turned on is the effective travelling length of bosons along the chain. As repulsion in the middle is tuned, bosons get to hop through longer distances and thereby their become more and more delocalized. The behaviour displayed by von Neumann entropy between both halves is consistent with a regime in which entanglement is being continuously redistributed across the system as a result of increasing hopping scope, but the fact that there is no turning point in Fig. 2 for CH indicates that such hopping never takes place across the complete length of the chain. Nevertheless, such hopping is enough to induce EEE at finite  $N$ , but not in the thermodynamic limit since EEE dies down against increasing chain size. In PTH chains, on the other hand, there exist a point in which hopping scope actually embraces the whole chain, which facilitates the particle transport from one end to the other, making the proportion of particles being held on the terminals useful for entanglement. Once this long scale hopping takes over, increasing the repulsion in intermediate sites reinforce end-to-end exchange and induces an increase in the amount of entanglement contained in the system, as can be seen in Figs. 2 and 3. At the same time, EEE begins to show a linear dependence with  $\zeta$  with a slope that is independent of the system size. In this case EEE remains even when the size of the chain is augmented, which means that long range correlations will manifest themselves in the thermodynamic limit.

## B. Dynamics

Here we investigate how EEE entanglement shows up as a result of dynamics in a chain initially prepared in a Mott insulating state. The typical behaviour of entan-

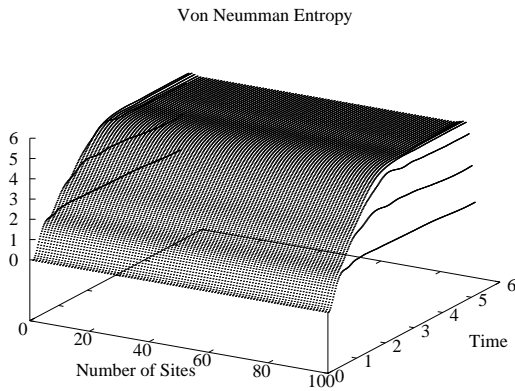


FIG. 4: Entanglement between complementary blocks in a chain with  $N = 100$  and  $U/J = 0.4$ . In this simulation  $\chi = 50$  and  $\delta t = 5 \times 10^{-5}$ . Entanglement saturates uniformly except close to the ends, where it displays smaller saturation values.

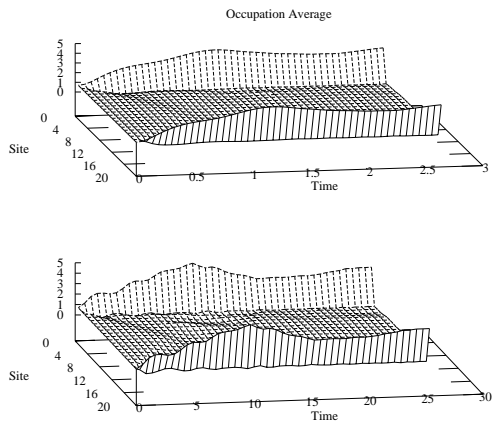


FIG. 5: Average number of bosons in chains with  $N = 20$  and  $M = 20$ .  $\chi = 50$ .  $U = 100$  for PTH (upper plot) and  $U = 200$  for CH (lower plot). Stronger repulsion constants are necessary in PTH chains in order to maintain intermediate sites fermionized so that no more than one particle can be at these sites. The initial state is a Mott insulator with one boson per site. At the beginning bosons start to migrate towards the ends, leaving the intermediate of the chain with half a boson per site on average. As a result of the hopping, EEE emerges after some time (Fig 6). For longer times slow oscillations can be seen, but the ends remain well populated.

gument in chains with homogeneous repulsion and hopping constants is shown in Fig. 4. As hopping is bigger than repulsion, particle tunnelling generates rich dynamics and entanglement behaves non-trivially in contrast to the high repulsion regime. Entanglement saturation is identical for all sites except those very close to the terminals, where saturation takes place at smaller values. Such boundary effects are typical of open chains [9, 31]. As a consequence, the ends are poorly entangled with the rest of system and between them as well. On the

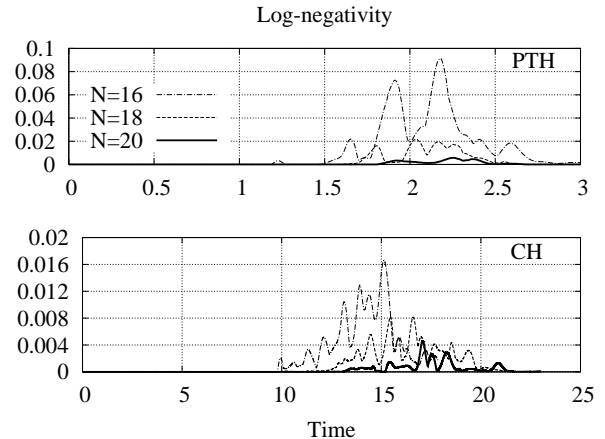


FIG. 6: EEE as a function of time for different chain sizes.  $\chi = 50$ .  $U = 100$  for CH and  $U = 200$  for PTH. The purpose is to restrain particle accumulation anywhere but the terminal sites. Entanglement in PTH chains is not only bigger but it also arises at early times than in CH chains. In both plots Log-negativity decreases with the size of the chain. Also, entanglement emerges well after bosons migrate to the ends (Fig 5).

other hand, dynamics in repulsionless chains is known to lead to a progressive thermalization of reduced density matrices of each site [32] and therefore any sort of two site entanglement is weak. In this sense, dynamic EEE in repulsionless chains is characteristically similar to that found previously in the ground state. As an alternative approach, we try the same methodology already applied and set all intermediate repulsion constants to high values in order to artificially create a particle distribution favourable to EEE. The effect on the average number of particles can be seen in Fig. 5. The ends get macroscopically occupied and tunnelling in intermediate places intensifies. EEE arises some time after the ends have been occupied (Fig. 6). In general, the bigger the chain the longer it takes for EEE to emerge. For PTH, a natural time scale is determined by the transmission period, namely  $T = \pi$  given our particular choice of  $\lambda$ . Entanglement arises after half of such period, just after information has got to travel from one end of the chain to the other, but there is not enough evidence that this is always the case, particularly for very long chains. Additionally, it is possible that entanglement will build up further for longer times, independently of the hopping profile, but this effect is difficult to observe as long time simulations require additional computational resources [28, 33].

### C. Perturbation approach and detection

We would now ideally like to generate such an entanglement between the ends where the logarithmic negativity exceeds unity (the maximum value in a two qubit state) so that the possibilities of multiple occupation numbers of

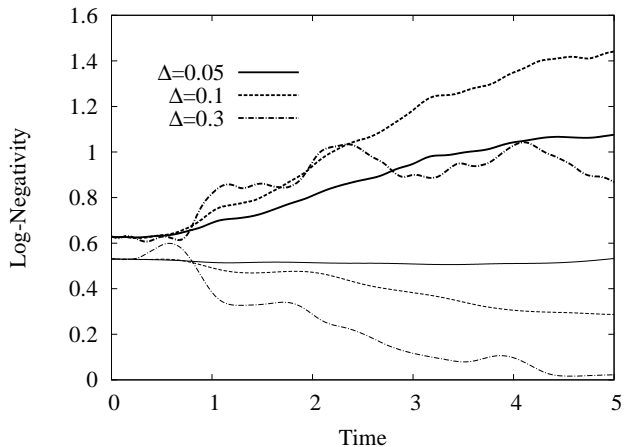


FIG. 7: EEE in a chain with  $N = 14$  and different values of  $\Delta$  for both CH and PTH. PTH lines are thicker than their CH equivalents. EEE in the ground state can be improved as a result of dynamics in PTH chains.  $\chi = 200$  for PTH and  $\chi = 100$  for CH.

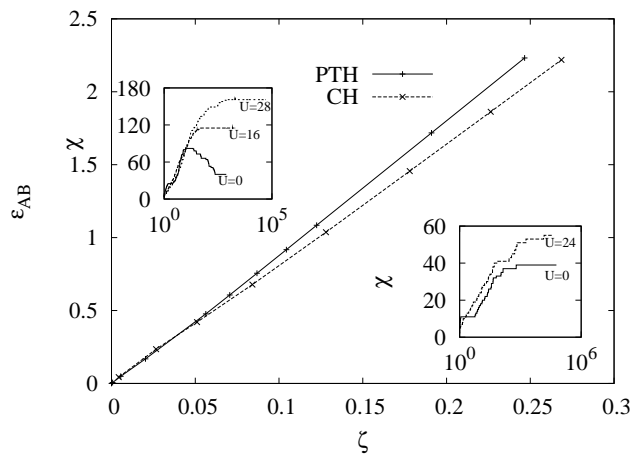


FIG. 8: Entanglement detection after bosons are sent through a 50:50 beamsplitter (see Ref. [34]). The original state is extracted from the ground state of chains with  $N=20$ . Insets: Ground state convergence using the TEBD algorithm for PTH (left top) and CH (right bottom) in chains with  $N = 20$ .

the ending sites is utilized highly beneficially. Looking at potential alternatives to the schemes discussed before, we now assume that a chain initially prepared in the ground state of a Hamiltonian with high intermediate repulsion and highly fermionized intermediate positions is set to evolve under the action of a small perturbation potential corresponding to a physical mechanism that internally pumps bosons in and out the ends. The idea is to use the perfect transmission properties at a perturbation level to generate entanglement as a result of transport. The quantum state at any time can be written as

$$|\psi(t)\rangle = e^{-it(\hat{H} + \Delta \sum_{j=1}^N \hat{h}_j)} |\psi_g\rangle, \quad (4)$$

where  $|\psi_g\rangle$  is the ground state of  $\hat{H}$ ,  $\Delta$  is a small number and  $\hat{h}_j$  represents a local operator acting on site  $j$ . For consistency, we require  $[\hat{H}, \sum_{j=1}^N \hat{h}_j] \neq 0$ . Here we consider that the local perturbations can be written as functions of the corresponding local number operator, i.e.  $h_j(\hat{N}_j)$ , where  $\hat{N}_j = \hat{a}_j^\dagger \hat{a}_j$ . We can establish a non-vanishing commutator between the perturbation and the Hamiltonian by choosing, for every site but the ends,  $h_j(x) = kx$ , where  $k$  is the integer distance between site  $j$  and the closest end. Notice that this is equivalent to considering a chain with spatially dependent chemical potential in intermediate positions. Moreover, the primary factor determining  $h_{1,N} = h$  is the optimization of boson-transfer from intermediate sites into the ends when an initial state  $|\psi_g\rangle$  is set. Supposing  $\langle \hat{H} \rangle$  remains stable during perturbation evolution and correlations between the Hamiltonian and the perturbation can be ignored, we can use the number-of-boson basis. In this way, performing average-energy balances among sequential particle distributions underlying an optimal trajectory we get

$$h(n_0 + \frac{1}{2}(\frac{N}{2} - k) + \frac{1}{2}) - h(n_0 + \frac{1}{2}(\frac{N}{2} - k)) = \frac{\Delta k}{2}, \quad (5)$$

where  $n_0$  is the average number of bosons allocated in one end at  $t = 0$ . After some algebraic manipulations we find  $h(x) = c_2 x^2 + c_1 x$  with  $c_1 = (\frac{N-1}{2} + 2n_0)\Delta$  and  $c_2 = -\Delta$ . With this perturbation, the mean number of bosons does not fluctuate much since the dynamics is still governed by a Hamiltonian with strong repulsion coefficients in intermediate sites and bosons remain squeezed into the ends. The leading mechanism in the evolution is the equitable exchange of particles between the terminals and the rest of the system. In addition, one can expect that such exchange will improve the communication between distant places and also the entanglement. Fig. 7 shows log-negativity as a function of time for different perturbation intensities. CH results are shown for comparative purposes. In the initial stages of evolution the dynamics is characterized by an increase of quantum fluctuations on the ends of the chain accompanied by little change in the average number of bosons. Hence, EEE is enhanced while avoiding massive migration of bosons towards the centre of the chain. Significantly, entanglement generation is improved not by adding interaction terms to the Hamiltonian but by adding a local perturbative potential.

Finally, we would like to comment about how this entanglement can be verified experimentally. Once the atoms condense in the ground state or after the dynamics has taken place, the detection scheme presented in [34] could be used. Following such a scheme, bosons on the ends are sent through a 50:50 beamsplitter and then the number of particles on the outputs is counted. Entanglement can then be detected using  $\epsilon_{AB} = tr(\hat{a}_c^\dagger \hat{a}_c \hat{\rho}) - \frac{N}{2} = tr(\hat{a}_1^\dagger \hat{a}_N \hat{\rho})$  where  $tr(\hat{a}_c^\dagger \hat{a}_c \hat{\rho})$  is the number of particles in

one output and  $\hat{\rho}$  is the reduced density matrix describing the ends.  $\epsilon_{AB} = 0$  for separable states and  $\epsilon_{AB} > 0$  for entangled states. In this way, entanglement is characterized in terms of experimentally measurable parameters. For illustrative purposes, we present in Fig. 8 a plot of  $\epsilon_{AB}$  obtained from the ground state of chains with PTH and CH. We conclude that  $\epsilon_{AB}$  correctly determines whether the state is entangled. In order to illustrate how our simulations converge to the ground state and the computational cost involved we also include plots of  $\chi$  against the number of steps. Here we emphasise that in our program  $\chi$  defines the dimension of an allocatable array which is being continuously resized according to the number of Schmidt coefficients in the canonical representation.

#### IV. SUMMARY

We have studied the ground state entanglement as well as the dynamical entanglement displayed by Bose-Hubbard chains for several configurations of parameters.

Our results indicate that chains with strong repulsion coefficients in intermediate places are suitable scenarios for the emergence of long scale hopping that can lead to a subsequent development in long-range quantum correlations. Entanglement also emerges as a result of dynamics in chains initially prepared in a Mott insulator state. In addition, we showed that ground state entanglement can be improved through perturbation dynamics. Irrespective of the issue of entanglement, the behaviours displayed by the ground and dynamical states that we have predicted for different repulsion profiles should be interesting to verify in an experiment. It would also be interesting to investigate how the transition from short scope to long scope hopping occurs. It could happen, and our results provide some evidence of this, that this transition is in fact a second order phase transition where EEE works as the order parameter.

JR acknowledges an EPSRC-DHPA scholarship. SB acknowledges support of the EPSRC, the EPSRC sponsored QIPIRC, the Royal Society and the Wolfson Foundation. We thank T.S. Monteiro and C. Hadley for very helpful comments.

- 
- [1] L. Campos Venuti, *et. al.*, Phys. Rev. Lett. **96**, 247206 (2006).
  - [2] J. Eisert, M. B. Plenio, S. Bose and J. Hartley **93**, 190402 (2004).
  - [3] M.-H. Yung and S. Bose, Phys. Rev. A **71**, 032310 (2005).
  - [4] D.I. Tsomokos, M.J. Hartmann, S.F. Huelga and M.B. Plenio New Journal of Physics **9**, 79 (2007).
  - [5] O. Romero-Isart, K. Eckert, C. Rodo and A. Sanpera, J. Phys. A: Math. Theor. **40** 8019 (2007).
  - [6] I. D'Amico, B. W. Lovett and T. P. Spiller, Phys. Rev. A **76**, 030302(R) (2007).
  - [7] L. Amico, R. Fazio, A. Osterloh and V. Vedral, Rev. Mod. Phys. **80**, 517 (2008).
  - [8] G. Vidal, Phys. Rev. Lett. **91**, 147902 (2003); G. Vidal, Phys. Rev. Lett. **93**, 040502 (2004); G. Vidal, Phys. Rev. Lett. **98**, 070201 (2007).
  - [9] R. Roth and K. Burnett, J. Phys. B: At. Mol. Opt. Phys. **37** 3893 (2004); T.D. Kuhner *et al*, Phys. Rev. B. **61**, 12474, (2000); S.R. White *et al*, Phys. Rev. B. **40**, 506, (1989).
  - [10] M. Moeckel and S. Kehrein, Phys. Rev. Lett. **100**, 175702 (2008); S. Gu *et al*, Phys. Rev. Lett. **93**, 086402 (2004); L. Tian *et al*, quant-ph/07052023.
  - [11] A.J. Daley *et al*, Phys. Rev. A **72**, 043618 (2005).
  - [12] M.B. Plenio *et al*, New J. Phys. **6**, 36 (2004).
  - [13] J.K. Stockton *et al*, Phys. Rev. A **67**, 022112 (2003).
  - [14] M.P.A. Fisher *et al*, Phys. Rev. B **40**, 546 (1989).
  - [15] D. Jaksch *et al*, Phys. Rev. Lett. **81**, 3108 (1998).
  - [16] M. Hild *et al*, Phys. Rev. A **76** 053614 (2007)
  - [17] M. Greiner *et al*, Nature **415**, 39 (2002).
  - [18] J.J. Chang, P. Engels and M.A. Hofer, Phys. Rev. Lett. **101**, 170404 (2008).
  - [19] T. Stoferle *et al*, Phys. Rev. Lett. **92**, 130403, (2004).
  - [20] S. Folling *et al*, Nature **448**, 1029 (2007).
  - [21] C. Simon, Phys. Rev. A **66**, 052323 (2002).
  - [22] L. Heaney, J. Anders, D. Kaszlikowski and V. Vedral, Phys. Rev. A **76** 053605 (2007); L. Heaney and J. Anders, arXiv:0810.2882.
  - [23] A.M. Rey *et al*, Phys. Rev. A **72**, 033616 (2005).
  - [24] I. Danshita and C. Clark, Phys. Rev. Lett. **102**, 030407 (2009); I. Danshita and P. Naidon, Phys. Rev. A **79**, 043601 (2009); R.V. Mishmash and L.D. Carr, arXiv:0710.0045.
  - [25] M. Christandl *et al*, Phys. Rev. Lett. **92**, 187902 (2004).
  - [26] S. Bose, Phys. Rev. Lett. **91**, 207901 (2003).
  - [27] M. Hartmann and M.B. Plenio, Phys. Rev. Lett. **100**, 070602 (2008).
  - [28] A. Perales and G. Vidal, Phys. Rev. A. **78**, 042337 (2008); A. Daley *et al*, J. Stat. Mech. P04005, (2004); H. Venzl *et al* arXiv:0808.3911.
  - [29] G. Vidal and R. Werner, Phys. Rev. A **65**, 032314 (2002).
  - [30] G. Vidal *et al*, Phys. Rev. Lett. **90**, 227902 (2003).
  - [31] A.M. Lauchli and C. Kollath, J. Stat. Mech. P05018, (2008).
  - [32] M. Cramer, C.M. Dawson, J. Eisert, T.J. Osborne, Phys. Rev. Lett. **100**, 030602 (2008); A. Flesch *et al*, cond-mat/08083779.
  - [33] T.J. Osborne, Phys. Rev. Lett **97**, 157202 (2006).
  - [34] J. Goold *et al*, arXiv:09022096.